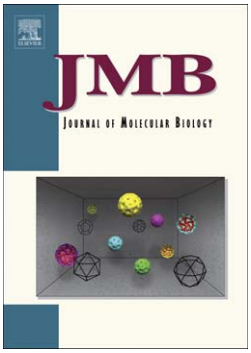

Structural Stability and Local Dynamics in Disease-Causing Mutants of Human Apolipoprotein A-I: What Makes the Protein Amyloidogenic?

Madhurima Das, Christopher J. Wilson, Xiaohu Mei, Thomas Wales, John R. Engen, Olga Gursky

PII: S0022-2836(15)00625-7
DOI: doi: 10.1016/j.jmb.2015.10.029
Reference: YJMBI 64906

To appear in: *Journal of Molecular Biology*

Received date: 18 September 2015
Revised date: 26 October 2015
Accepted date: 27 October 2015

Please cite this article as: Das, M., Wilson, C.J., Mei, X., Wales, T., Engen, J.R. & Gursky, O., Structural Stability and Local Dynamics in Disease-Causing Mutants of Human Apolipoprotein A-I: What Makes the Protein Amyloidogenic?, *Journal of Molecular Biology* (2015), doi: 10.1016/j.jmb.2015.10.029

Structural Stability and Local Dynamics in Disease-Causing Mutants of Human Apolipoprotein A-I: What Makes the Protein Amyloidogenic?

10/26/2015

Madhurima Das,[a*] Christopher J. Wilson,[b*] Xiaohu Mei,[a] Thomas Wales,[b] John R. Engen,[b] and Olga Gursky[a]

Affiliations:

[a] Department of Physiology & Biophysics, Boston University School of Medicine, 700 Albany Street, Boston, MA 02118, USA

[b] Department of Chemistry & Chemical Biology, Northeastern University, 360 Huntington Avenue, Boston, MA 02115, USA

* MD and CW contributed equally to this work

Corresponding author:

Olga Gursky, Department of Physiology & Biophysics, Boston University School of Medicine, W329a, 700 Albany St., Boston, MA 02118, USA Phone: 617-638-7894; FAX: 617-638-4041; E-mail: Gursky@bu.edu

ABSTRACT

ApoA-I, the major protein of plasma high-density lipoprotein, removes cellular cholesterol and protects against atherosclerosis. ApoA-I mutations can cause familial amyloidosis, a life-threatening disease wherein N-terminal protein fragments form fibrils in vital organs. To unveil the protein misfolding mechanism and to understand why some mutations cause amyloidosis while others do not, we analyzed the structure, stability and lipid-binding properties of naturally occurring mutants of full-length human apoA-I causing either amyloidosis (G26R, W50R, F71Y, L170P) or aberrant lipid metabolism (L159R). Global and local protein conformation and dynamics in solution were assessed by circular dichroism, fluorescence, and hydrogen-deuterium exchange mass spectrometry. All mutants showed increased deuteration in residues 14-22, supporting our hypothesis that decreased protection of this major amyloid "hot spot" can trigger protein misfolding. In addition, L159R showed local helical unfolding near the mutation site, consistent with cleavage of this mutant in plasma to generate the labile 1-159 fragment. Together, the results suggest that reduced protection of the major amyloid "hot spot", combined with structural integrity of the native helix-bundle conformation, shift the balance from protein clearance to β-aggregation. A delicate balance between the overall structural integrity of a globular protein and the local destabilization of its amyloidogenic segments may be a fundamental determinant of this and other amyloid diseases. Furthermore, mutation-induced conformational changes observed in the helix bundle, which comprises N-terminal 75% of apoA-I, and its flexible C-terminal tail suggest the propagation of structural perturbations to distant sites via an unexpected template-induced ensemble-based mechanism, challenging the classical structure-based view.

Highlights

- Cardioprotective protein apoA-I can cause amyloid disease via an unknown mechanism
- Disease-causing mutations decrease the protection of the main amyloidogenic segment
- Structural integrity of the native fold may shift the balance towards misfolding
- Local unfolding near an interhelical linker targets the protein for degradation
- Mutational effects propagate to distant sites via an ensemble-based mechanism

Abbreviations:

apoA-I – apolipoprotein A-I; AApoAI – familial apoA-I amyloidosis; HDL – high-density lipoprotein, ANS – anilino-8-naphthalenesulfonate; DMPC - 1,2-dimyristoyl-*sn*-glycero-3-phosphocholine; CD – circular dichroism; HDX MS – hydrogen-deuterium exchange mass spectrometry.

Key words:

Protein stability and misfolding; protein-lipid interactions; high-density lipoprotein; hydrogen-deuterium exchange mass spectrometry; transmission of conformational changes; familial amyloidosis and atherosclerosis

INTRODUCTION

Protein misfolding and deposition as insoluble fibers is a hallmark of amyloidoses. These potentially life-threatening diseases, which can affect the central nervous system (in Alzheimer's, Parkinson's and prion diseases) or other vital organs (in systemic amyloidoses), have limited treatment options and no cure. Among more than 40 polypeptides that have been implicated in amyloidoses, the apolipoprotein (apo) family is overrepresented, probably because these dynamic proteins possess high hydrophobicity and low structural stability, which are necessary for their function but also promote β-aggregation.[1,2] Apolipoproteins are lipid-surface-binding proteins that solubilize lipids and transport them in aqueous environments such as plasma. Dissecting molecular pathways of apolipoprotein misfolding, from the native highly α-helical conformation to the cross-β-sheet in amyloid, is an unresolved fundamental problem whose solution may help guide the search for the much-needed therapies. Here, we explore the misfolding mechanism of apoA-I, the major protein of plasma high-density lipoprotein (HDL).

HDLs (a.k.a. "good cholesterol") are 8-12 nm nanoparticles comprised of proteins and lipids, which transport cholesterol from peripheral cells to the liver.[3] ApoA-I (243 residues) comprises ~70% of the total HDL protein and forms a structural scaffold and a functional ligand on the particle surface. ApoA-I and HDL possess a range of cardioprotective properties.[3,4] Although ~95% of plasma apoA-I circulates in a stable α-helical conformation bound to HDL,[5-7] ~5% forms a labile lipid-poor/lipid-free monomer,[8,9] termed "free" for brevity (Fig. 1A). Free apoA-I is a transient species that rapidly binds to lipoproteins or is recruited to the plasma membrane for HDL biogenesis. Alternatively, free apoA-I can be either degraded by yet-to-be-identified proteases or misfolds and deposits as fibrils in two human diseases. Familial apoA-I amyloidosis (AApoAI) is an autosomal dominant disorder in which fragments 1-83 to 1-100 of mutant apoA-I deposit as fibrils in vital organs (kidney, liver, heart, etc.) and damage them.[10-12] In acquired amyloidosis, which has emerged as a common contributing factor to atherosclerosis, non-variant full-length apoA-I deposits as fibrils in arterial plaques.[12-20] Such fibril deposition is cytotoxic, activates arterial macrophages and decreases plaque stability, thus contributing to atherogenesis.[15,19,20]

Fig. 1

Previously, we mapped AApoAI mutations on the atomic structure of free human Δ(185-243)apoA-I, a C-terminally truncated protein that contains all ~20 known AApoAI mutation sites.[21] This structure comprises an approximate 4-helix bundle encompassing the N-terminal 75% of apoA-I.[7] The location of the mutation sites suggested that they destabilize the helix bundle and weaken protein-lipid interactions, thus promoting apoA-I misfolding.[21] Surprisingly, biophysical studies of the naturally occurring mutants of human apoA-I (including two AApoAI variants, G26R and W50R) showed that large global destabilization of free or lipid-bound apoA-I is neither necessary nor sufficient for amyloidosis.[22] Therefore, additional factors must be involved in AApoAI, perhaps including local structural perturbations in apoA-I.

Bioinformatics analysis identified four 4- to 9-residue hydrophobic segments, particularly residues 14-22 (LATVYVDVL), with high sequence propensity to trigger amyloid formation.[22-25] These amyloid "hot spots" are normally protected from misfolding by their native α-helical structure in free (Fig. 1B) or lipid-bound apoA-I. We hypothesized that reduced protection of these hot spots upon mutations or other modifications promotes apoA-I misfolding. This idea underlies the first proposed molecular mechanism of apoA-I misfolding in familial and acquired amyloidosis.[22] According to this mechanism, perturbed packing of amyloid hot spots triggers their conversion from the native α-helix to a parallel intermolecular β-zipper that propagates from the N- to the C-terminus, culminating in amyloid formation either by the full-length protein (in acquired amyloidosis) or its N-terminal 9-11 kDa segment (in AApoAI). In this mechanism, protein misfolding was proposed to precede proteolysis in AApoAI, although alternative pathways in which misfolding and proteolysis occur in parallel could not be excluded.[2]

To test key aspects of the proposed misfolding mechanism, here we explored the structure, stability and lipid-binding properties of several naturally occurring disease-causing mutants of full-length human apoA-I. These include F71Y (the most conservative AApoAI mutation) and L170P (one of the "outside" AApoAI point mutations that cluster in residues 170-178 located outside the 9-11 kDa N-terminal segments found in amyloid deposits). Both F71Y and L170P sites are located in the "bottom" half of the helix bundle where most other AApoAI mutations are clustered.[21] Analysis of these mutants extends our previous stability studies of two AApoAI mutations, G26R and W50R, located in the "middle" of the helix bundle[22] (Fig. 1B). As a non-amyloidogenic control, we studied L159R variant and the 1-159 fragment, which is generated

upon proteolysis of this variant in plasma.[26] L159R mutation impedes HDL maturation, leading to lack of α-migrating HDL and an increased risk of atherosclerosis.[26,27] We used a battery of biophysical methods to determine the effects of these mutations on the local backbone conformation and dynamics in solution. The results help explain what makes the protein amyloidogenic and provide surprising insights into the propagation of conformational changes to distant sites in this highly dynamic protein.

RESULTS

Mutations Influence Protein Structure and Stability in Solution

First, we tested the effects of AApoAI (F71Y and L170P) and non-AApoAI mutations (L159R) on the secondary structure of free protein at 25 °C. Far-UV CD spectra of WT and mutant apoA-I superimposed at 200-250 nm indicating ~50% α-helical content (determined with 5% accuracy) (Fig. 2A). Decreased CD signal at 185-200 nm indicated mutation-induced disordering. Mutants G26R and W50R showed similar but smaller effects.[22] Next, CD melting data were recorded to test protein stability (Fig. 2B). In F71Y, the melting temperature T_m (measured with 2 °C accuracy) decreased by 5 °C compared to WT, indicating a small destabilization upon mutation. Comparable destabilization was seen in W50R and G26R (δT_m=-3 °C).[22] L159R and L170P showed not only much larger destabilization (δT_m=-11 °C) but also a 2-fold decrease in the transition steepness at T_m. The van't Hoffs enthalpy of unfolding decreased accordingly, from about 40 kcal/mol for WT and F71Y to about 20 kcal/mol for L159R and L170P, indicating a 2-fold decrease in the unfolding cooperativity (discussed below). Fig. 2

The mutational effects on the aromatic packing in free proteins were probed by near-UV CD at 25 °C (Fig. 2C). Bundle-forming residues 1-184 contain all four Trp (W8, W50, W72 and W108) and five out of seven Tyr in apoA-I (Y18, Y29, Y100, Y115, Y166), while the remaining two (Y192 and Y236) are located in the flexible C-terminal tail. Therefore, near-UV CD of free full-length apoA-I reports on the tertiary structure in the helix bundle.[7] WT showed a downward-pointing peak at 295 nm with a shoulder at 285 nm, which is dominated by Trp with a contribution from Tyr, and bands at 255-280 nm coming from Tyr and Phe (Fig. 2C, black). Human plasma apoA-I[28,29] (Fig. 2D, black) and in its 1-184 fragment[7] have a similar spectrum,

which is a signature of native aromatic packing in the helix bundle. The bundle contains two aromatic clusters at the bottom (W8, F71, W72) and the top (F33, F104, W108), and π-cation interactions at the bottom (W8, R61) and in the middle (W50, K23).[7] G26R, W50R and F71Y caused marked changes in near-UV CD, which is not surprising since these mutations involve a Trp removal (W50R) or directly interfere with the aromatic packing in the middle (G26R) or the bottom (F71Y) of the bundle. Unexpectedly, L159R and L170P showed the largest spectral changes, with more negative CD signal at 255-280 nm and an upward pointing peak at 293 nm (Fig. 2C). Intriguingly, similar spectra are characteristic of normal human plasma HDL (Fig. 2D, red) and of model lipoproteins containing apoA-I.[29,30] Consequently, L159R and L170P mutations mimic lipid-induced changes in the aromatic packing of non-variant apoA-I.

ApoA-I binding to lipid involves opening of the helix bundle, probably along the cleft between the two pairs of helices (Fig. 1B),[7] to form an antiparallel helical "double belt" on HDL surface.[6] The remarkable similarity between the near-UV CD spectra of HDL-bound non-variant apoA-I (Fig. 2D, red) and lipid-free L170P and L159R mutants (Fig. 2C, pink and violet) suggests that these mutations in the apolar core of the helix bundle increase the cleft between the helix pairs (Fig. 1B). A two-fold decrease in the unfolding cooperativity of L159R and L170P mutants supports this idea and suggests that cooperative units in these mutants contain two helices instead of four in WT and F71Y (Fig. 2B).

The local environment of the tryptophan residues in the helix bundle was assessed by intrinsic Trp fluorescence (Fig. 2E). The wavelength of the maximal fluorescence in all proteins was circa 338 nm, typical of Trp largely buried in an apolar environment. G26R, W50R, and F71Y mutations caused relatively little spectral changes. Surprisingly, L159R and L170P showed a small but significant increase in the emission intensity, which was particularly pronounced at the excitation wavelength λ_{ex}=280 nm where both Tyr and Trp absorb. Such increased emission may possibly reflect: i) reduced Trp quenching by the solvent; ii) reduced Trp self-quenching upon widening the cleft between the helix pairs, which is expected to disrupt the packing of W8 and W72 against each other in the aromatic cluster at the bottom of the helix bundle[7]; and/or iii) increased energy transfer from Tyr to Trp in L159R and L170P mutants. Although the emission spectra containing contributions from all four Trp did not allow us to

differentiate these effects, the invariant wavelength of maximal fluorescence indicates that the average local polarity around these Trp residues was not affected by mutations.

To compare the solvent-accessible hydrophobic surfaces in free proteins, 1-anilino-8-naphthalenesulfonate (ANS) fluorescence spectra were recorded. ANS is an apolar fluorescent probe that binds to large solvent-accessible hydrophobic cavities, which are found in molten-globular folding intermediates but generally not in fully folded or fully unfolded globular proteins in solution. ANS binding increases its fluorescence emission due to decreased quenching by the solvent. Free WT apoA-I has low structural stability, high aggregating propensity and other molten-globular properties[28] and binds ANS,[31] causing increased emission (Fig. 2F). Compared to the WT, slightly destabilized mutants F71Y, W50R and G26R showed slightly increased ANS emission. This is perhaps not surprising, as less stable globular proteins tend to have greater solvent-accessible hydrophobic surface. Surprisingly, L159R and L170P, which are even more destabilized, showed decreased ANS emission (Fig. 2E), which we attribute to the better-ordered and less solvent-accessible conformation of the hydrophobic C-terminal tail in these two mutants (discussed below). The observation of the greatly reduced ANS binding in the C-terminally truncated Δ(185-243)apoA-I (data not shown) supports this interpretation and indicates that the C-terminal tail provides the major but not the sole ANS binding site in apoA-I.

In summary, spectroscopic studies showed that the mutations produce little disorder in the secondary structure of free apoA-I at 25 °C. G26R, W50R, and F71Y show slightly reduced thermal stability (δT_m=-3°C to -5 °C) and slightly altered aromatic packing (Fig. 2B). L159R and L170P are not only much less stable (δT_m=-11 °C) but also show a 2-fold decrease in the unfolding cooperativity (Fig. 2B) and HDL-like aromatic packing (Fig. 2C, D), suggesting an increased cleft separating two pairs of helices in the 4-helix bundle (Fig. 1B). Other distinct properties of the two "outside" mutants include increased Trp emission and decreased ANS binding (Fig. 2E, F). Thus, the mutations fall into two groups: mildly destabilizing "inside" mutations (W50R, G26R and F71Y) and strongly destabilizing "outside" mutations (L170P and L159R). The latter include the non-amyloidogenic variant, L159R. These results support our idea that global structural destabilization in solution is neither necessary nor sufficient to make the protein amyloidogenic. Therefore, additional factors are likely important in AApoAI, including local dynamics and proteolysis, as well as protective protein-lipid interactions.

Mutations Influence Protein-Lipid Interactions

To determine how lipid interactions with apoA-I were affected by the mutations, mutant proteins were studied in the context of apoA-I:DMPC complexes, which are used as simple models of nascent HDL (Fig. 3). Clearance of DMPC liposomes (diameter d>100 nm) by apoA-I variants to form HDL-size particles (d~10 nm) at 24 °C was monitored by turbidity. G26R, L159R and L170P had no significant effect on the time course of clearance, while F71Y (Fig. 3A) and W50R slightly accelerated it.[22] The latter probably reflects local effects of aromatic substitutions rather than global protein destabilization, which was relatively small in F71Y (Fig. 2) or absent in W50R.[22] Non-denaturing gel electrophoresis and negative stain electron microscopy showed that all mutant proteins formed similar-size lipoproteins (11-12 nm) that mimic nascent "discoidal" HDL (Fig. 3B, C). Far-UV CD indicated 70-74% α-helix content in these lipoproteins (Fig. 3D). The melting data showed that the mutations decreased lipoprotein stability (Fig. 3E). The apparent T_m, which was determined from the first derivative of the CD heating data recorded at a scan rate of 11 °C/h as previously described,[32] decreased from $T_{m,app}$=83 °C for DMPC complexes with WT to 78.5 °C (F71Y), 74 °C (L170P), or 67 °C (L159R). DMPC complexes with W50R or G26R showed little destabilization.[22]

Fig. 3

In summary, the mutations did not impair the ability of apoA-I to bind model phospholipid and remodel it into HDL-like complexes, nor did they alter the size or secondary structure of these complexes. However, the mutations decreased the lipoprotein stability in the order of WT ≥ W50R ≥ G26R > F71Y > L170P > L159R. The largest destabilization was observed in the two "outside" mutants, L170P (AApoAI) and particularly L159R (non-AApoAI). In contrast, the common AApoAI mutation W50R did not significantly destabilize the lipoproteins.[22] If a mutation in apoA-I destabilizes plasma HDL, it is expected to shift the population distribution from the lipid-bound (protected) to free (labile) apoA-I, and thereby potentially augment amyloidosis.[21,22] However, our results suggest that such destabilization is neither necessary (W50R) nor sufficient (L159R) for amyloidosis.

Mutations Influence Local Conformation and Dynamics in the Helix Bundle

To monitor the effects of the mutations on the local backbone conformation and dynamics, each protein was probed with HDX MS. Figure 4 shows the time course of deuterium uptake for representative polypeptide regions, and Supplemental Figures S1 and S2 show the summary of the data, which have 96% completeness and 4.4 redundancy. Increased deuteration indicates less extensive H-bonding and/or higher solvent accessibility, a direct result of changes to protein fluctuations.[33]

In the N-terminal half of apoA-I (residues 1-121 encompassing helices I-III from the 4-helix bundle), large mutation-induced changes were observed in residues 14-22 (Fig. 4B, C), which are predicted to form the major amyloid hot spot.[2,22-25] In the crystal structure, these residues form a well-ordered kinked helical segment in the middle of the helix bundle (Fig. 1B, blue), which is consistent with the slow deuteration of this segment observed in the WT (Fig. 4B, C, black; also see [34]). The mutant proteins had greatly increased deuteration in the 14-22 segment; the order of protection from exchange was WT > F71Y > W50R > G26R > L159R ≥ L170P (Fig. 4B, C). This order supports the hypothesis that perturbed native packing in residues 14-22 can trigger apoA-I misfolding.[22] However, the non-amyloidogenic L159R mutant also showed greatly reduced protection in residues 14-22. Therefore, reduced structural protection of the major amyloid hot spot is not sufficient to cause amyloidosis.

Fig. 4

The HDX MS data also showed a similar rank order of protection for other largely α-helical N-terminal segments (Fig. 4D, G, H, I), including those overlapping a minor amyloid hot spot 69-73 (Fig. 4G), as well as residues 76-104 (Fig. 4H, I) which encompass the cleavage sites 83-93 associated with AApoAI.[10-12,21] Chetty and colleagues reported that G26R has reduced protection at these sites and proposed that this helps generate the proteolytic fragment 1-83 found in AApoAI deposits.[35] Our results reveal that, although AApoAI mutations G26R and L170P greatly reduce (although do not eliminate) protection from exchange in the 83-93 region, the non-amyloidogenic mutation L159R has a similar or even larger effect (Fig. 4H, I). The latter observation suggests that reduced protection of segment 83-93, which was proposed to facilitate cleavage followed by amyloid deposition of the N-terminal fragment of G26R apoA-I,[35] does not always cause AApoAI. Moreover, AApoAI mutations W50R and F71Y caused minimal increases in deuteration in residues 83-93, suggesting that these variants retain their well-ordered α-helical conformation similar to WT (Fig. 4H, I, orange and green). Therefore, contrary to the

prevailing notion, amyloid formation by at least some AApoAI mutants, such as F71Y and W50R, does not result from local α-helical unfolding causing enhanced cleavage in positions 83 to 93. Together, these results support the idea that apoA-I misfolding in AApoAI can precede cleavage in such mutants as F71Y and W50R; hence, fragments 1-83 to 1-93, which are found in AApoAI deposits *in vivo*, are not necessarily the causative agents of the disease, but perhaps its end products generated upon cleavage of the misfolded full-length protein ([17,22] and references therein). Still, cleavage of other AApoAI mutants, such as L170P and G26R, may potentially occur in parallel or even prior to their misfolding. These events could perhaps be deconvoluted more definitively once the proteases cleaving apoA-I in vivo have been identified.

Interestingly, no significant effects of mutations were detected in residues 44-57, which showed high levels of deuteration in all proteins (Fig. 4E, F). These residues contain an extended β-strand-like segment 44-55 observed in the crystal structure,[21] which overlaps with a minor predicted amyloid hot spot 53-58[22,36] (Fig. 1). Although the extended segment 44-55 is largely polar and is predicted not to have high amyloidogenic potential,[2] it was proposed to facilitate α-helix to β-sheet conversion,[17,21] and peptide fragments encompassing this segment can form amyloid fibrils *in vitro*.[17,23,25] Lack of mutational effects in the HDX of segment 44-55 (Fig. 4E, F) suggests that changes to the native state of this largely unprotected segment[34] do not occur on the time scale of labeling used here, or do not occur at all. Hence, although segment 44-55 may potentially contribute to apoA-I misfolding, it is unlikely to trigger AApoAI.

To summarize, HDX MS revealed that most α-helical segments in the N-terminal half of apoA-I have a rank order of protection of WT > F71Y > W50R > G26R >> L170P, L159R. Although the rank order of global protein stability determined by CD was somewhat different, WT ≥ W50R > G26R > F71Y >> L170R ≥ L159R (Fig. 2B and [22]), all data consistently show that L170P and L159R mutations cause the largest local and global perturbations in the helix bundle.

Central Linker Holds Clues to Non-amyloidogenic Behavior of L159R

Interestingly, our HDX data showed that the rank order of protection in apoA-I variants is different for the N-terminal half, the central linker, and the C-terminal tail (Fig. 4). Important

clues are provided by the central region that contains a flexible linker in residues 121-142 (helical repeat H5 out of 11 11/22-mer amino acid sequence repeats in apoA-I[37]) and adjacent residues. In the crystal structure of Δ(185-243)apoA-I, this central linker is highly flexible (backbone B-factors ~80 Å^2) and probably facilitates domain swapping of helix IV (residues 143-184) in the 4-helix bundle during dimer-to-monomer conversion[7] (circular arrow in Fig. 1B). On HDL, parts of repeats 5 and 6 were proposed to form a flexible loop encompassing residues 134-146 that can dissociate from the lipid.[38,39] Consistent with this inherent flexibility, all proteins showed relatively low protection (high levels of deuteration) in this region (Fig. 4K-O) (also see [34]).

Importantly, L159R showed markedly reduced protection in repeat H6 (residues 143-164) near the mutation site as compared to all other proteins explored (Fig. 4M-O). In fact, this was the only region showing a large difference between this non-amyloidogenic mutant and its amyloidogenic counterpart, L170P (for additional evidence see Figure 6A below). We propose that in L159R, loss of protection in this dynamic region makes it labile to proteolysis. Basic residue pair R159, R160 formed upon mutation may also augment proteolysis, since basic pairs are preferred substrates for certain proteases that are thought to cleave apoA-I *in vivo*.[26] Transgenic mouse studies showed that human L159R apoA-I (but not WT) in plasma is cleaved by an unknown protease to generate an approximate 1-159 proteolytic fragment.[26] This fragment was proposed to be structurally unstable and undergo rapid degradation *in vivo*.[26,27]

To test the idea that cleavage near L159R produces a structurally labile fragment, we analyzed the structure and stability of the recombinant 1-159 fragment. The CD data of free protein showed that, although this fragment lacks the disordered C-terminal tail, it is only 40% α-helical at 25 °C suggesting loss of a large part of the helix bundle structure (Fig. 5A). HDX MS data revealed that, compared to full-length proteins, the 1-159 fragment shows decreased protection in its terminal residue segments 1-70 and 125-159, suggesting substantial helical unfolding in these segments (Fig. 5D-G and K; light-blue and brown line in Fig. 5C). However, the 1-159 fragment retains protection in residues 72-103 (Fig. 5H, I, J), implying a substantially intact helix III (gray ribbon in Fig. 5C). These results indicate that cleavage of full-length L159R apoA-I near the mutation site, which removes the C-terminal tail and a part of helix IV from the bundle, destabilizes the remaining helices, particularly the rest of helix IV and helices I and II

Fig. 5

(brown and light-blue, Fig. 5C); the latter encompass the region with the highest amyloidogenic propensity in apoA-I.[22] Loss of ordered structure in this region is expected to greatly accelerate its proteolytic degradation. The melting data of 1-159 fragment revealed T_m=43 °C and indicated only ~30% α-helical content at 37 °C (Fig. 5B). Similarly, reduced helical content and reduced stability were observed in DMPC complexes with 1-159 fragment as compared to the full-length protein (data not shown), suggesting that deletion of the C-terminal part in this protein decreases its affinity for lipid. Collectively, these results suggest that local helical unfolding near the mutation site, followed by enhanced proteolysis in this region, probably target L159R apoA-I for degradation by generating a structurally labile substantially unfolded 1-159 fragment. Such a local unfolding followed by degradation would explain why L159R apoA-I does not form amyloid *in vivo* despite decreased protection of its major amyloid hot spot (Fig. 4B, C).

Effects of Mutations on the EX1/EX2 Exchange Kinetics

The kinetics of HDX provide additional insights into local protein conformation and dynamics. Two kinetic regimes, EX1 and EX2, have been observed in proteins.[33,40] In EX2, which is predominant in most globular proteins, progressive deuteration occurs upon multiple unfolding/refolding events because the rate of local refolding is faster than that of the HDX reaction. EX2 manifests itself as a unimodal spectrum with the peak position gradually shifting towards higher mass (higher deuteration) as a function of time. In EX1, the deuteration occurs though a cooperative unfolding event where local refolding is slower than the HDX reaction. EX1 kinetics manifests itself as a bimodal spectral distribution (when the alternative conformations are sufficiently separated on the m/z scale) or as spectral broadening (when they are close in m/z), with the lower-mass peak corresponding to the protected conformation and higher-mass peak to the unprotected one. EX1 generally indicates less stable local structure and/or coexistence of alternative conformations. Free apoA-I shows substantial EX1 kinetics[34] (Figs. 6A and S3), consistent with its dynamic molten globule-like structure.[28]

Figure 6 summarizes the EX1/EX2 kinetics analyses in the current study. Fig. 6A shows typical mass spectra for deuteration of peptide 125-158 in WT and mutants of apoA-I; other example peptides are in Fig S3. All mass spectra for all peptides were monitored for EX1/EX2 and the results are summarized in Fig. 6B according to the half-life of EX1 kinetics. In WT, Fig. 6

EX1 occurs mainly in three regions: residues 114-147 containing the central linker (121-142) and adjacent groups; residues 212-229 and 234-243 from the C-terminal tail; and residues 33-42 overlapping the linker between helix bundle segments I and II. This result is in excellent agreement with the x-ray crystal structure of Δ(185-243)apoA-I showing high flexibility in these regions.[7]

Similar to WT, all mutants showed high EX1 in residues 114-147 encompassing the central linker, and in C-terminal residues 212-219. In addition, distinct effects of mutations on EX1 were observed (Fig. 6B, C). First, all mutants showed much faster EX1 in two regions: one overlapping the N-terminal amyloid hot spot 14-22, and another around residues 29-46 overlapping the linker between the helix bundle segments I and II. All mutants also showed faster EX1 in residues 57-71 at the "bottom" of the helix bundle. Further, some amyloidogenic (L170P, G26R) and non-amyloidogenic (L159R) mutants showed more rapid EX1 in residues 72-103 overlapping the AApoAI cleavage sites, while other amyloidogenic mutants (F71Y, W50R) showed little changes. These results support our idea that increased flexibility at these sites is neither necessary nor sufficient for AApoAI. Interestingly, L159R and particularly L170P showed decreased or no EX1 at the C-terminal tail, consistent with our idea that the flexible C-terminal tail in these two mutants is better packed against the helix bundle (described below).

EX1 exchange kinetics provides important clues on local conformational changes near the mutation site in L159R. MS spectra of the long peptic peptide 125-158 clearly showed a bimodal distribution in WT, G26R, W50R, F71Y, and L170P variants (Fig. 6A). This result reflects the presence of two alternative conformations observed previously in this segment:[7,34] a flexible linker overlapping residues 125-142 is likely the part showing fast deuteration, while the stable α-helix in residues 143-158 is likely responsible for slow deuteration. Supporting this idea are the data for shorter fragments within this region: peptides 125-136 and 125-147 show rapid EX1 kinetics (deep-green in Fig. 6B) while peptide 148-158 indicates EX2 kinetics and general protection from exchange (white, Fig. 6B). In 125-158 peptide, the bimodal distribution was observed during at least 1 min of exchange in WT and in all AApoA-I mutants, and up to 10 min in L170P (Fig. 6A). In a striking contrast, the L159R variant and 1-159 fragment showed a unimodal distribution reaching near-maximal deuteration after 5 s of exchange, indicating just one unprotected conformation in this region. These results very strongly support the idea of local

helical unfolding near the mutation site in L159R and 1-159 fragment; in contrast, all other full-length proteins retained helical structure in this region. Together, these EX1/EX2 data further support our interpretation of the mutational effects on the local conformation and dynamics in free apoA-I, including local helical unfolding near the mutation site in L159R variant.

Propagation of Conformational Changes to Distant Sites

Another surprising result was the propagation of the conformational changes from the mutation sites in the helix bundle to the C-terminal tail (residues 185-243). In WT, the flexible C-terminal tail has low protection[34] and is thought to interact weakly with the helix bundle ([7,9,41] and refs. therein). HDX MS data showed that F71Y and W50R mutations have little effect on the deuteration of the C-terminal tail, while G26R slightly increases it (Fig. 4T-V). Surprisingly, L159R and L170P significantly decrease deuteration in the C-terminal tail (Fig. 4T-V), except for its very end (Fig. 4W), suggesting more extensive packing of the tail against the helix bundle. This conclusion is supported by decreased EX1 kinetics observed in the C-terminal tail of L159R and L170P (Fig. 6).

Our spectroscopic studies help explain this observation. The "HDL-like" aromatic packing in free L170P and L159R detected by near-UV CD (Fig. 2C, D), together with a large destabilization of these mutants and a 2-fold decrease in their unfolding cooperativity observed by far-UV CD (Fig. 4B), suggest an increased cleft separating the two pairs of helices in the helix bundle (Fig. 1B). We posit that widening of this narrow hydrophobic cleft helps to accommodate the hydrophobic C-terminal tail in L170P and L159R mutants. Sequestration of the C-terminal tail in the cleft is expected to compete with ANS binding at these hydrophobic sites, which explains reduced ANS binding observed in L170P and L159R (Fig. 2F). Such sequestration is also expected to improve shielding from solvent quenching of the four Trp in the helix bundle, which may explain increased Trp emission observed in L170P and L159R (Fig. 2E). Other contributions to this increased Trp emission may result from the energy transfer from the two Tyr in the C-terminal tail (Y192, Y136) to the Trp in the helix bundle (W8, W50, W72, W108), and perhaps from decreased Trp self-quenching upon increasing the cleft in the helix bundle in L170P and L159R.

In summary, the results of HDX MS, far-and near-UV CD, ANS binding and Trp fluorescence, together with the crystal structure of Δ(185-243)apoA-I, reveal how mutation-induced local perturbations in the core of the ordered helix bundle in the N-terminal part of the protein shift the conformational equilibrium in the flexible C-terminal tail. Such a template-induced shift in the conformational equilibrium of the disordered region is akin to the newly developed concepts of the ensemble nature of allostery, which challenge the classic structure-based view on propagation of conformational changes to distant sites.[42]

DISCUSSION

Summary of the Mutational Effects on the Conformation of Free ApoA-I

Our results reveal the effects of several disease-causing point mutations on the local and global structure and dynamics of full-length lipid-free human apoA-I. HDX MS data show that, although the overall protein fold is retained, each mutation elicits distinct structural responses in the helix bundle and the C-terminal tail. First, L170P and L159R show higher deuteration and faster EX1 kinetics in the bundle-forming α-helices, yet lower deuteration and slower or no EX1 in the C-terminal tail (Fig. 4, A-J and S-W). We attribute these effects to the enhanced hydrophobic interactions between the flexible tail and the helix bundle cleft that is widened in these two "outside" mutants. Second, L159R mutant is the only protein that shows increased deuteration in the linker region adjacent to the mutation site, which reflects local helical unfolding near this site upon substitution of the hydrophobic Leu159 with charged Arg in the core of the helix bundle (Fig. 4 M-O, stars).

Some mutations (L159R, L170P and G26R) cause increased disorder in the well-ordered α-helical segment 83-93 that is cleaved in AApoAI deposits, while others (F71Y, W50R) do not. This suggests that cleavage at these sites may be secondary to protein misfolding, at least in some AApoAI mutants (F71Y, W50R), supporting the idea that the apoA-I misfolding can precede proteolysis at these sites ([17,22] and references therein). Therefore, such proteolysis may be the end result of AApoAI rather than its cause, or perhaps the misfolding and proteolysis may occur in parallel. This conclusion is consistent with the misfolding of full-length apoA-I observed in acquired amyloidosis.

Finally, segment 44-55 that adopts a β-strand-like conformation in the crystal structure of Δ(185-243)apoA-I[21] remains invariant upon mutations (Fig. 4E). Consequently, although this segment may possibly be involved in α-helix to β-sheet conversion in apoA-I, it probably does not trigger AApoAI.

What Makes the Protein Amyloidogenic?

Our results help better understand what makes apoA-I amyloidogenic. We posit that WT apoA-I is protected from misfolding by sequestering the major amyloid hot spot 14-22 in the middle of the helix bundle (Fig. 1B, blue). Previously we proposed that reduced protection of this sensitive segment upon mutations or other modifications can trigger its conversion into an intermolecular β-sheet.[22] Our HDX MS data support this idea and reveal that one of the major effects of all disease-causing mutations explored here is decreased protection in residues 14-22 (Fig. 4B, C). However, this effect alone does not always cause amyloidosis, as L159R does not form amyloid *in vivo* despite greatly reduced protection in residues 14-22 (Fig. 4B, C). We propose that the *in vivo* behavior of L159R mutant is probably due to its rapid proteolytic degradation after cleavage near the mutation site. Such cleavage to generate an approximate 1-159 fragment was observed in plasma,[26] and our HDX MS data suggest that this cleavage is facilitated by local helical unfolding near 159R (Fig. 4M-O, stars). Structural analysis suggests that cleavage at residue 159 deletes a large part of one helix from the 4-helix bundle and generates a labile 1-159 fragment that is largely unfolded at near-physiologic conditions, with only ~30% α-helix content at 37 °C and T_m=43°C (Fig. 5, top panels). As a result of substantial unfolding of helices I, II and IV detected by HDX MS (Fig. 5, bottom panels), a 1-159 fragment is expected to be rapidly degraded in plasma, which would likely target L159R mutant for rapid degradation *in vivo*. In contrast, all AApoAI mutants studied here, including L170P whose overall conformation and stability closely resemble those of L159R, have intact structure in their interhelical linker (Fig. 4, central part) and hence, retain their native helix bundle conformation long enough to initiate β-aggregation.

Our results suggest that two factors are necessary to make apoA-I amyloidogenic: i) reduced protection of the major amyloid hot spot (residues 14-22), and ii) its presentation in the context of the native helix-bundle structure whose life time is sufficient to augment protein aggregation

rather than rapid clearance. Mutational effects on protein secretion levels, which were observed in several naturally occurring apoA-I mutants[43] including L159R,[26,27] are also expected to influence the disease. Future studies will test whether similar factors influence apoA-I misfolding and amyloid deposition upon other mutations or pathogenic modifications, such as Met oxidation in acquired amyloidosis.[17,18]

In summary, large overall destabilization of the native protein structure is not necessarily amyloidogenic, as it can not only reduce the protection of the amyloid hot spots but also accelerate protein degradation as well as impair its generation. This competition between protein generation, clearance and misfolding helps explain why the extent of overall structural destabilization in apoA-I and other amyloidogenic proteins (e. g. transthyretin and immunoglobulin light chain) does not always correlate with amyloid formation *in vivo*.[22,44-46] The delicate balance between the protein generation, proteolysis and aggregation, which depends, in part, on the local backbone conformation and dynamics in the amyloid hot spots versus protease-sensitive regions, is probably a fundamental determinant for globular protein misfolding and amyloid deposition *in vivo*.

In addition, mutation-induced conformational changes observed in the helix bundle and in the flexible C-terminal tail of apoA-I suggest the propagation of mutation-induced structural perturbations to distant sites via a template-induced ensemble-based mechanism. Similar to free apoA-I whose interactions between the globular N-terminal and dynamic C-terminal domains have been well documented,[7,9,41,47] other large lipid-free apolipoproteins such as apoE or apoA-IV also form important interactions between their N- and C-terminal domains.[2,48,49] It is tempting to speculate that the conformational ensembles in these proteins, particularly in apoE that, like apoA-I, is comprised of a helix bundle and a long flexible hydrophobic C-terminal tail, may be modulated via a similar template-induced ensemble-based mechanism. If so, such a mechanism may possibly contribute to the distinct effects of apoE isoforms (which differ in Cys/Arg substitutions in the helix bundle) in neurodegenerative disease ([2,48] and references therein).

MATERIALS and METHODS

Recombinant proteins were expressed and purified to ~95% purity as previously described.[7] Complexes of proteins with model lipid dimyristoyl phosphatodylcholine (DMPC) were obtained

by liposome clearance at 24 °C using 1:4 protein:lipid weight ratio and following established protocols.[9,22] The time course of DMPC clearance was monitored by turbidity using Varian Cary-300 spectrometer as described.[22] Lipoprotein size and morphology were characterized by non-denaturing PAGE and negative-stain transmission electron microscopy following published protocols.[9,22] Far- and near-UV circular dichroism (CD) spectra and the melting data were recorded from free proteins or lipoproteins using an AVIV 430 spectropolarimeter as described previously.[9,22] Proteins' α-helical content and the effective enthalpy of unfolding were determined from far-UV CD data as described.[28] Emission spectra of Trp and 1-anilino-8-naphthalenesulfonate (ANS) were recorded from free proteins using FluoroMax spectrofluorimeter following published protocols.[31] Hydrogen deuterium exchange mass spectrometry (HDX MS) was performed on free proteins essentially as described previously[50] using 55 μg/ml protein concentration at which apoA-I is fully monomeric.[29] Further details of the experiments, including Figures S1-S3 showing additional aspects of HDX MS data, are provided in the Supplementary Material. All experiments were repeated 2-5 times to ensure reproducibility.

SUPPLEMENTARY MATERIAL Experimental details concerning sample preparation and spectroscopic analyses, and Figures S1–S3 showing additional HDX MS data. This material is available free of charge via the Internet.

ACKNOWLEDGEMENTS We are indebted to Donald L. Gantz for help with electron microscopy. We are grateful to colleagues in Physiology & Biophysics at Boston University School of Medicine for useful discussions. This work was supported by the National Institutes of Health grants GM067260 (to O.G.) and GM101135 (to J. E.), with additional support from Waters Corporation (J. E.). X.M. was supported by the NIH grant HL116518.

Figure Legends

Figure 1 Model representation of apoA-I structure.

(A) Cartoon showing apoA-I and HDL. Each HDL particle contains 2-5 copies of apoA-I and polar lipids (mainly phospholipids and cholesterol) on the surface, and apolar lipids (mainly cholesterol ester and triacylglycerol) in the core. ApoA-I on HDL adopts an antiparallel helical "double-belt" conformation.[5,6] ApoA-I can dissociate from HDL in a labile monomeric free form that can: i) rapidly bind to other lipoproteins or generate new HDL ([8,9] and refs. therein), ii) get degraded or iii) misfold.

(B**)** Amyloid "hot spots" and mutation sites mapped on the proposed structure of apoA-I monomer. The structure was obtained from the dimer observed in the 2.2 Å crystal structure of Δ(185-243)apoA-I (PDB ID 3R2P) via the domain swapping of helix IV residues 143-184 around the dimer 2-fold (circular arrow).[7] The flexible C-terminal tail (residues 185-243, drawn by line) was absent from the crystallized construct. Disease-causing point substitutions explored in the current study are indicated. Residue segments that were proposed to be important for amyloidosis are indicated: 14-22 (blue) is the major predicted amyloid "hot spot"; 53-58 (teal) and 69-72 (yellow) are weakly predicted amyloid "hot spots"; 44-55 is the sole β-strand-like segment in the crystal structure; 83-93 contain the cleavage sites generating 1-83 to 1-93 fragments found in AApoAI deposits; and 227-232 (red) is the predicted C-terminal amyloid "hot spot".[21-25] The latter segment overlaps the α-helix forming the primary lipid binding site.

Figure 2 Conformation and stability of free full-length apoA-I variants analyzed by spectroscopy.

(A) Effects of mutations on the secondary structure assessed by far-UV CD at 25 °C. Insert shows SDS PAGE.

(B) Effects of mutations on the structural stability assessed by far-UV CD. Melting data were recorded at 222 nm to monitor α-helical unfolding during heating at a constant rate from 5 to 95 °C. Dotted lines indicate melting temperatures, T_m.

(C) Aromatic packing assessed by near-UV CD at 25 °C.

(D) Near-UV CD spectra of non-variant human plasma apoA-I and HDL are shown for comparison.

(E) Intrinsic Trp fluorescence of apoA-I variants. The emission spectra were recorded using an excitation wavelength of 280 nm.

(F) ANS binding to apoA-I variants assessed by fluorescence at 25 °C. The spectrum for ANS in protein-free buffer is shown for comparison.

Figure 3 Biophysical characterization of model "discoidal" HDL reconstituted from DMPC and mutant apoA-I. Protein to lipid ratio in all preparations was 1:4 mg/mg.

(A) Time course of DMPC liposome clearance by apoA-I monitored by turbidity.

(B) Non-denaturing gel electrophoresis of variant apoA-I:DMPC complexes; free proteins are shown for comparison.

(C) Negative-stain electron micrographs of the apoA-I:DMPC complexes. Most "discoidal" particles are seen stacked on edge.

(D) Far-UV CD spectra of apoA-I:DMPC complexes.

(E) CD melting data recorded at 222 nm of apoA-I:DMPC complexes upon heating and cooling from 5 to 95 °C at a rate of 11 °C/hour. Dashed lines indicate apparent melting temperatures that decreased from $T_{m,\,app}$=83 °C for WT to 78.6°C (F71Y), 74 °C (L170P), and 67 °C (L159R).

Figure 4 Time course of deuterium uptake for selected regions of lipid-free monomeric apoA-I variants measured by HDX MS. The peptide map showing all peptic fragments of apoA-I followed by HDX is in Supplementary material (Fig. S1) as is a one-page comparison of differences in deuteration across all apoA-I variants (Fig. S2).

Figure 5 Conformation and stability of lipid-free 1-159 fragment of human apoA-I. Far-UV CD spectra (A) and the melting data (B) were recorded as in Figure 2. (C) Structural model depicting conformation of the 1-159 fragment inferred from the x-ray crystal structure of the 1-184 fragment (PDB ID 3R2P) and our HDX MS data. (D-K) Representative deuteration curves of 1-159 fragment compared to full-length WT and variant apoA-I. At near-physiologic conditions, a substantial part of the native helical structure is lost in 1-159 fragment (C). HDX data in panels D-G and K suggest that this helical loss occurs mainly in residues 1-70 and 125-159 (light blue and brown, C).

Figure 6 Comparison of EX1/EX2 kinetics in specific regions of WT and variant apoA-I.

(A) Representative isotopic envelopes of the peptic peptide 125-158. The deuterium labeling times are indicated; "und" is undeuterated state. Bimodal isotope patterns indicative of EX1 kinetics are seen at early incubation times in the WT and AApoAI variants G26R, W50R, F71Y, and L170P, suggesting that the peptide contains two regions differing in protection. L159R and 1-159 show unimodal patterns with $t_{½}$ <5 s, suggesting low protection for the whole peptide.

(B) Location and time scale of EX1 kinetics. Each horizon

tal line represents an apoA-I variant; 11 helical repeats, G* and H1-H10,[37] in the sequence of apoA-I are shown at the top. Peptide mass spectra (illustrated in panel A and Figure S3) were inspected for EX1/EX2 kinetics. For peptides with EX1 kinetics, the half-life of unfolding, $t_{½}$, was measured and color coded as shown. Peptides with EX2 kinetics or very slow (>>240 min) EX1 kinetics are in white.

(C) Several peptides exhibiting EX1 kinetics mapped onto the model structure of Δ(185-243)apoA-I monomer.

REFERENCES

1. Teoh, C. L., Griffin, M. D., Howlett, G. J. (2011). Apolipoproteins and amyloid fibril formation in atherosclerosis. *Protein Cell 2(2)*, 116-127.
2. Das, M., Gursky, O. (2015) Amyloid-forming properties of human apolipoproteins: Sequence analyses and structural insights. *Adv. Exp. Med. Biol. 855*, 175-211.
3. Rothblat, G. H., Phillips, M. C. (2010) High-density lipoprotein heterogeneity and function in reverse cholesterol transport. *Curr. Opin. Lipidol. 21*, 229-238.
4. Navab, M., Reddy, S.T., Van Lenten, B. J., Fogelman, A. M. (2011) HDL and cardiovascular disease: atherogenic and atheroprotective mechanisms. *Nat. Rev. Cardiol. 8(4)*, 222–232.
5. Borhani, D. W., Rogers, D. P., Engler, J. A., Brouillette, C. G. (1997) Crystal structure of truncated human apolipoprotein A-I suggests a lipid-bound conformation. *Proc. Natl. Acad. Sci. USA 94(23)*, 12291-12296.
6. Brouillette, C. G., Anantharamaiah, G. M., Engler, J. A., Borhani, D. W. (2001) Structural models of human apolipoprotein A-I: a critical analysis and review. *Biochim. Biophys. Acta 1531(1-2)*, 4-46.
7. Mei, X., Atkinson, D. (2011) Crystal structure of C-terminal truncated apolipoprotein A-I reveals the assembly of HDL by dimerization. *J. Biol. Chem. 286(44)*, 38570-38582.
8. Rye, K. A., Barter, P. J. (2004) Formation and metabolism of prebeta-migrating, lipid-poor apolipoprotein A-I. *Arterioscler. Thromb. Vasc. Biol. 24*, 421–428.
9. Jayaraman S., Cavigiolio G., Gursky O. (2012) Folded functional lipid-poor apolipoprotein A-I obtained by heating of high-density lipoproteins: Relevance to HDL biogenesis *Biochem. J. 442(3)*, 703-712.
10. Obici, L., Franceschini, G., Calabresi, L., Giorgetti, S., Stoppini, M., Merlini, G., Bellotti, V. (2006) Structure, function and amyloidogenic propensity of apolipoprotein A-I. *Amyloid 13(4)*, 191−205.
11. Rowczenio, D., Dogan, A., Theis, J. D., Vrana, J.A., Lachmann, H.J., Wechalekar, A.D., Gilbertson, J.A., Hunt, T., Gibbs, S.D., Sattianayagam, P.T., Pinney, J.H., Hawkins, P.N., Gillmore, J.D. (2011) Amyloidogenicity and clinical phenotype associated with five novel mutations in apolipoprotein A-I. *Am. J. Pathol. 179(4)*, 1978−1987.
12. Ramella, N.A., Schinella, G.R., Ferreira, S.T., Prieto, E.D., Vela, M.E., Ríos, J.L., Tricerri, M.A., Rimoldi, O.J. 2012 Human apolipoprotein A-I natural variants: Molecular mechanisms underlying amyloidogenic propensity. *PLoS One 7(8)*, e43755.

13. Ramella, N.A., Rimoldi, O.J., Prieto, E.D., Schinella, G.R., Sanchez, S.A., Jaureguiberry, M.S., Vela, M.E., Ferreira, S.T., Tricerri, M.A. (2011) Human apolipoprotein A-I-derived amyloid: Its association with atherosclerosis. *PLoS One 6(7)*, e22532.
14. Mucchiano, G.I., Haggqvist, B., Sletten K., Westermark, P. (2001) Apolipoprotein A-1-derived amyloid in atherosclerotic plaques of the human aorta. *J. Pathol. 193(2)*, 270–275.
15. Röcken, C., Tautenhahn, J., Bühling, F., Sachwitz, D., Vöckler, S., Goette, A., Bürger, T. (2006) Prevalence and pathology of amyloid in atherosclerotic arteries. *Arterioscler. Thromb. Vasc. Biol. 26*, 676–677.
16. Howlett, G.J., Moore, K.J. (2006) Untangling the role of amyloid in atherosclerosis. *Curr. Opin. Lipidol.* 17(5): 541-547.
17. Wong, Y. Q., Binger, K. J., Howlett, G. J., Griffin, M. D. (2010) Methionine oxidation induces amyloid fibril formation by full-length apolipoprotein A-I. *Proc. Natl. Acad. Sci. USA 107(5)*, 1977-1982.
18. Chan, G.K., Witkowski, A., Gantz, D.L., Zhang, T.O., Zanni, M.T., Jayaraman, S., Cavigiolio, G. (2015) Myeloperoxidase-mediated methionine oxidation promotes an amyloidogenic outcome for apolipoprotein A-I. *J. Biol. Chem. 290(17)*, 10958-10971.
19. Lepedda, A.J., Cigliano, A., Cherchi, G.M., Spirito, R., Maggioni, M., Carta, F., Turrini, F., Edelstein, C., Scanu, A.M., Formato, M. (2009) A proteomic approach to differentiate histologically classified stable and unstable plaques from human carotid arteries. *Atherosclerosis 203(1)*, 112-118.
20. Patel, S., Chung, S.H., White, G., Bao, S., Celermajer, D.S. (2010) The "atheroprotective" mediators apolipoprotein A-I and Foxp3 are over-abundant in unstable carotid plaques. *Int. J. Cardiol. 145(2)*, 183-187.
21. Gursky, O., Mei, X., Atkinson, D. (2012) Crystal structure of the C-terminal truncated apolipoprotein A-I sheds new light on the amyloid formation by the N-terminal segment. *Biochemistry 51(1)*, 10-18.
22. Das, M., Jayaraman, S., Mei, X., Atkinson, D., Gursky, O. (2014) Amyloidogenic mutations in human apolipoprotein A-I are not necessarily destabilizing: A common mechanism of apoA-I misfolding in familial amyloidosis and atherosclerosis. *FEBS J. 281(11)*, 2525-2542.
23. Mendoza-Espinosa P., Montalvan-Sorrosa D., García-González V., Moreno A., Castillo R., Mas-Oliva J. (2014) Microenvironmentally controlled secondary structure motifs of apolipoprotein A-I derived peptides. *Mol. Cell. Biochem. 393(1-2)*, 99-109.

24. Adachi, E., Kosaka, A., Tsuji, K., Mizuguchi, C., Kawashima, H., Shigenaga, A., Nagao, K., Akaji, K., Otaka, A., Saito, H. (2014) The extreme N-terminal region of human apolipoprotein A-I has a strong propensity to form amyloid fibrils. *FEBS Lett. 588(3)*, 389-394.

25. Louros, N. N., Tsiolaki, P. L., Griffin, M. D., Howlett, G. J., Hamodrakas, S. J., Iconomidou, V. A. (2015) Chameleon 'aggregation-prone' segments of apoA-I: A model of amyloid fibrils formed in apoA-I amyloidosis. *Int. J. Biol. Macromol.* 79, 711-718.

26. McManus, D. C., Scott, B. R., Franklin, V., Sparks, D. L., Marcel, Y. L. (2001) Proteolytic degradation and impaired secretion of an apolipoprotein A-I mutant associated with dominantly inherited hypoalphalipoproteinemia. *J. Biol. Chem*. *276(24),* 21292-21302.

27. Sorci-Thomas, M. G., Zabalawi, M., Bharadwaj, M. S., Wilhelm, A. J., Owen, J. S., Asztalos B. F., Bhat, S., Thomas, M. J. (2012) Dysfunctional HDL containing L159R ApoA-I leads to exacerbation of atherosclerosis in hyperlipidemic mice. *Biochim. Biophys. Acta 1821(3),* 502-512.

28. Gursky, O., Atkinson, D. (1996) Thermal unfolding of human high-density apolipoprotein A-1: Implications for a lipid-free molten globular state. *Proc. Natl. Acad. Sci. USA 93(7),* 2991-2995.

29. Leroy, A., Toohill, K. L., Fruchart, J. C., Jonas, A. (1993) Structural properties of high density lipoprotein subclasses homogeneous in protein composition and size. *J. Biol. Chem. 268(7),* 4798-4805.

30. Gao, X., Jayaraman, S., Guha, M., Wally, J., Lu, M., Atkinson, D., Gursky, O. (2012) Application of circular dichroism to lipoproteins: Structure, stability and remodeling of good and bad cholesterol. *In: Circular Dichroism: Theory and Spectroscopy,* D.S. Rogers, Edt. *Nova Publishers* pp. 175-215.

31. Gorshkova, I. N., Mei, X., Atkinson, D. (2014) Binding of human apoA-I[K107del] variant to TG-rich particles: implications for mechanisms underlying hypertriglyceridemia. *J. Lipid Res. 55(9),* 1876-1885.

32. Gursky, O., Ranjana, Gantz, D. L. (2002) Complex of human apolipoprotein C-1 with phospholipid: thermodynamic or kinetic stability? *Biochemistry 1(23)*, 7373-7384.

33. Englander, S. W., Kallenbach, N. R. Hydrogen exchange and structural dynamics of proteins and nucleic acids. *Q. Rev. Biophys*. (1983) 16(4), 521-655.

34. Chetty, P. S., Mayne, L., Lund-Katz, S., Stranz, D., Englander, S. W., Phillips, M. C. (2009) Helical structure and stability in human apolipoprotein A-I by hydrogen exchange and mass spectrometry. *Proc. Natl. Acad. Sci. USA 106,* 19005–19010.

35. Chetty, P. S., Ohshiro, M., Saito, H., Dhanasekaran, P., Lund-Katz, S., Mayne, L., Englander, W., Phillips, M. C. (2012) Effects of the Iowa and Milano mutations on apolipoprotein A-I structure and dynamics determined by hydrogen exchange and mass spectrometry. *Biochemistry 51(44)*, 8993-9001.
36. Wong, Y. Q., Binger, K. J., Howlett, G. J., Griffin, M. D. (2012) Identification of an amyloid fibril forming peptide comprising residues 46-59 of apolipoprotein A-I. *FEBS Lett. 586(13)*, 1754-1758.
37. Segrest, J. P., Jones, M. K., De Loof, H., Brouillette, C. G., Venkatachalapathi, Y. V., Anantharamaiah, G. M. (1992) The amphipathic helix in the exchangeable apolipoproteins: a review of secondary structure and function. *J. Lipid Res.* 33(2), 141-166.
38. Maiorano, J. N., Jandacek, R. J., Horace, E. M., Davidson, W. S. (2004) Identification and structural ramifications of a hinge domain in apolipoprotein A-I discoidal high-density lipoproteins of different size. *Biochemistry 43(37)*, 11717-11726.
39. Martin, D. D., Budamagunta, M. S., Ryan, R. O., Voss, J. C., Oda, M. N. (2006) Apolipoprotein A-I assumes a "looped belt" conformation on reconstituted high density lipoprotein. *J. Biol. Chem. 281(29)*, 20418-20426.
40. Roder, H, Wagner, G, Wüthrich, K. (1985) Amide proton exchange in proteins by EX1 kinetics: studies of the basic pancreatic trypsin inhibitor at variable p2H and temperature. *Biochemistry 24(25)*, 7396-7407.
41. Segrest, J. P., Jones, M. K., Shao, B., Heinecke, J. W. (2014) An experimentally robust model of monomeric apolipoprotein A-I created from a chimera of two X-ray structures and molecular dynamics simulations. *Biochemistry 53(48)*, 7625-7640.
42. Motlagh, H. N., Wrabl, J. O., Li, J., Hilser, V. J. (2014) The ensemble nature of allostery. *Nature 508(7496)*, 331-339.
43. Sorci-Thomas, M. G., Thomas, M. J. (2002) The effects of altered apolipoprotein A-I structure on plasma HDL concentration. *Trends Cardiovasc. Med. 12(3)*, 121-128.
44. del Pozo Yauner, L., Ortiz, E., Sanchez, R., Sanchez-Lopez, R., Guereca, L., Murphy, C.L., Allen, A., Wall, J.S., Fernandez-Velasco, D.A., Solomon, A., Becerril, B. (2008) Influence of the germline sequence on the thermodynamic stability and fibrillogenicity of human lambda 6 light chains. *Proteins 72*, 684–692.
45. Shnyrov, V.L., Villar, E., Zhadan, G.G., Sanchez-Ruiz, J.M., Quintas, A., Saraiva M.J., Brito, R.M. (2000) Comparative calorimetric study of non-amyloidogenic and amyloidogenic variants of the homotetrameric protein transthyretin. *Biophys. Chem. 88(1-3)*, 61-67.

46. Klimtchuk, E.S., Gursky, O., Patel, R.S., Laporte, K.L., Connors, L.H., Skinner, M., Seldin, D.C. (2010) The critical role of the constant region in thermal stability and aggregation of amyloidogenic immunoglobulin light chain. *Biochemistry 49(45)*, 9848-9857.

47. Koyama, M., Tanaka, M., Dhanasekaran, P., Lund-Katz, S., Phillips, M.C., Saito, H. (2009) Interaction between the N- and C-terminal domains modulates the stability and lipid binding of apolipoprotein A-I. *Biochemistry 48(11)*, 2529-2537.

48. Frieden, C., Garai, K. (2012) Structural differences between apoE3 and apoE4 may be useful in developing therapeutic agents for Alzheimer's disease. *Proc. Natl. Acad. Sci. USA 109(23)*, 8913-8918.

49. Walker, R.G., Deng, X., Melchior, J.T., Morris, J., Tso, P., Jones, M.K., Segrest, J.P., Thompson, T.B., Davidson, W.S. (2014) The structure of human apolipoprotein A-IV as revealed by stable isotope-assisted cross-linking, molecular dynamics, and small angle x-ray scattering. *J. Biol. Chem. 289(9)*, 5596-5608.

50. Morgan, C. R., Hebling, C. M., Rand, K. D., Stafford, D. W., Jorgenson, J. W., Engen, J. R. (2011) Conformational transitions in the membrane scaffold protein of phospholipid bilayer nanodiscs. *Mol. Cell Proteomics 10(9)*, M111.

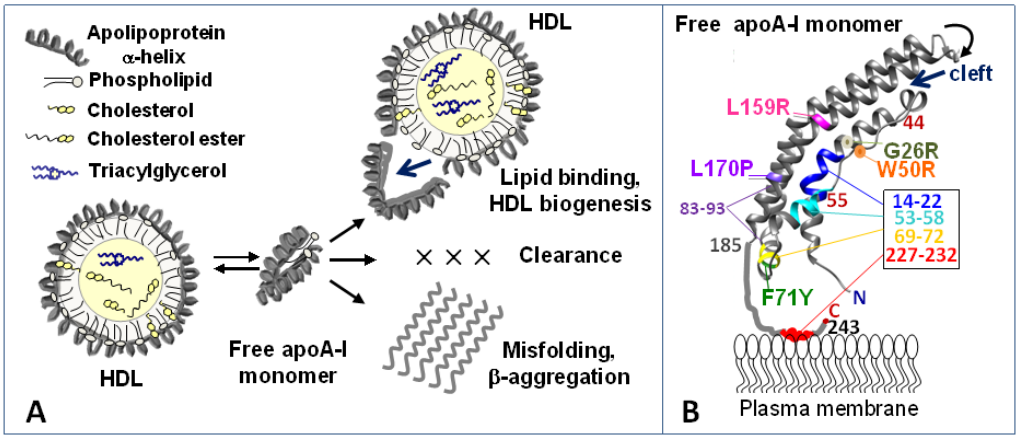

Figure 1

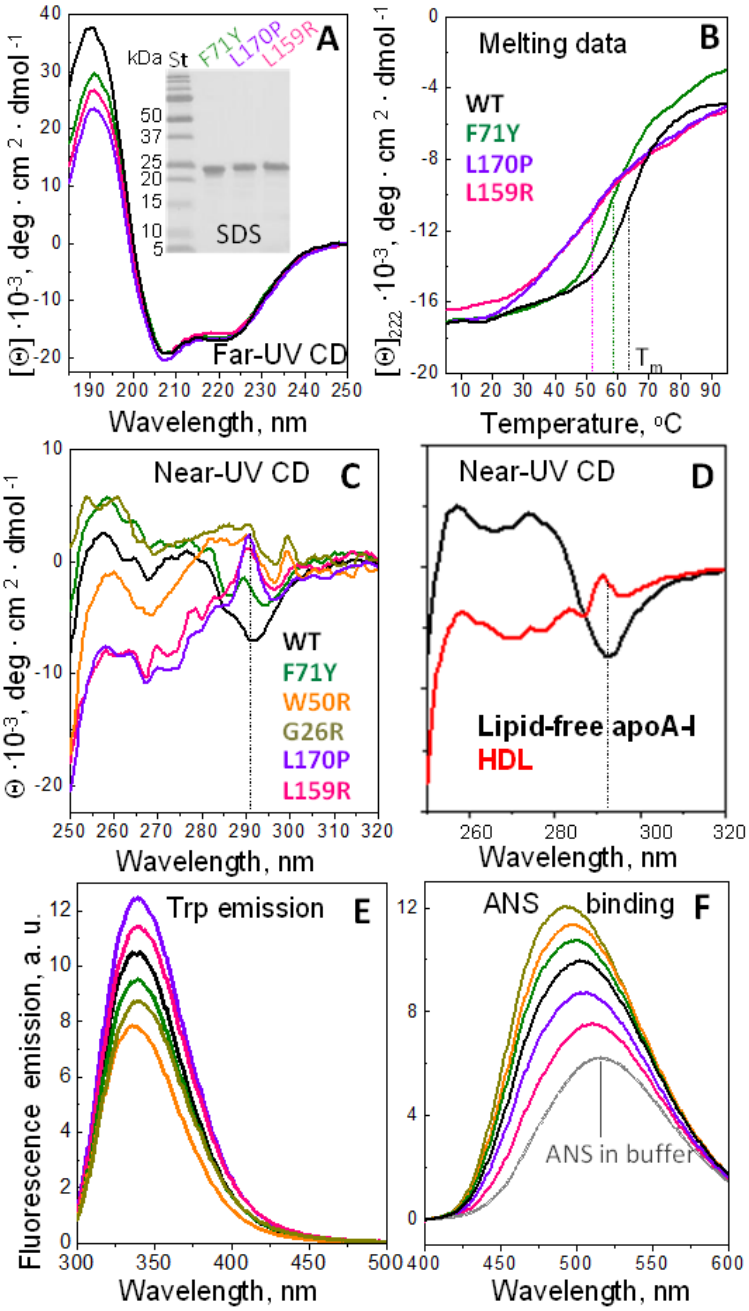

Figure 2

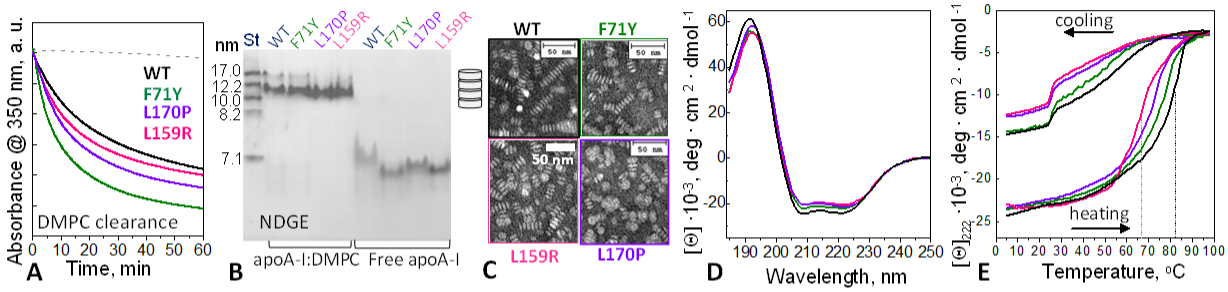

Figure 3

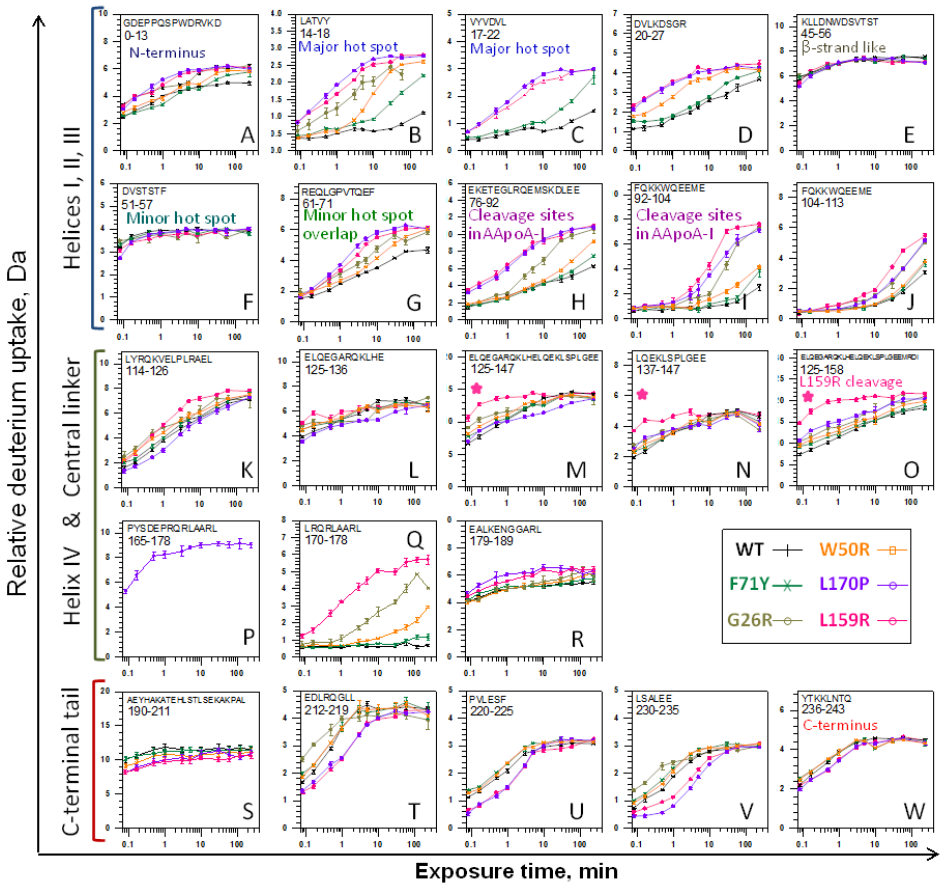

Figure 4

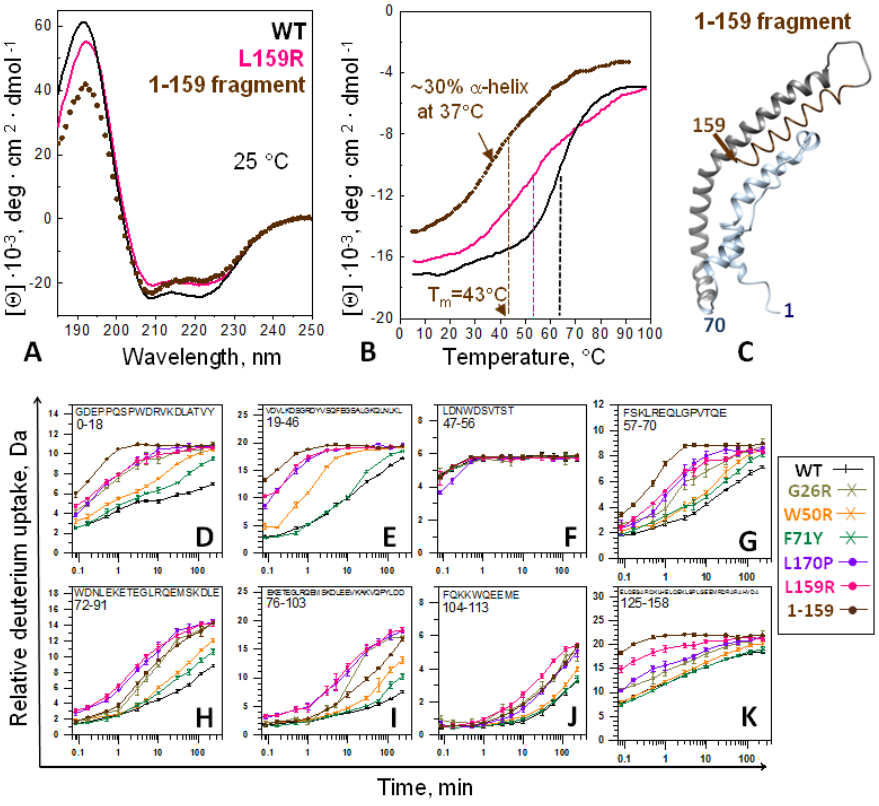

Figure 5

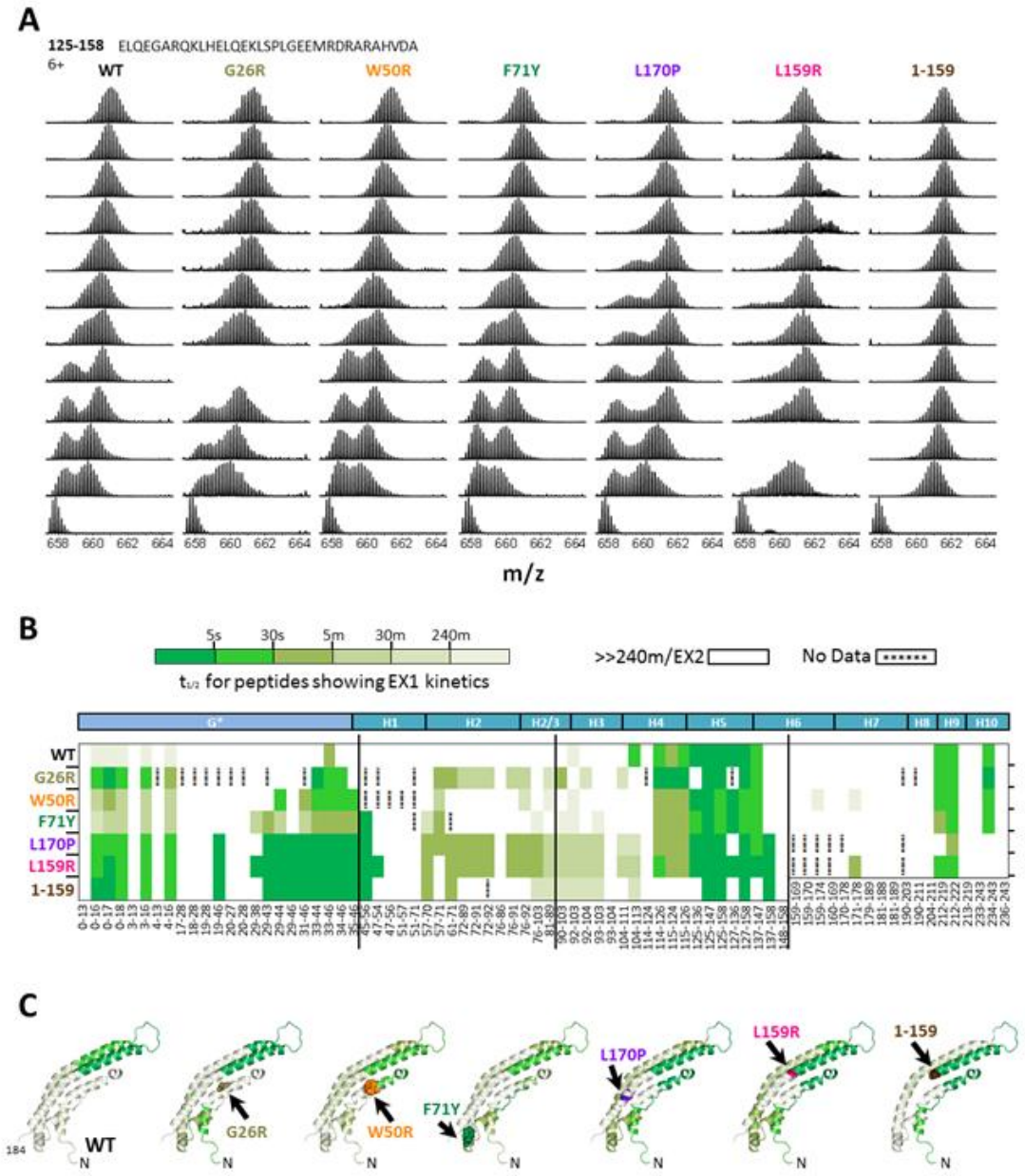

Figure 6

Table Of Contents / Abstract Graphics

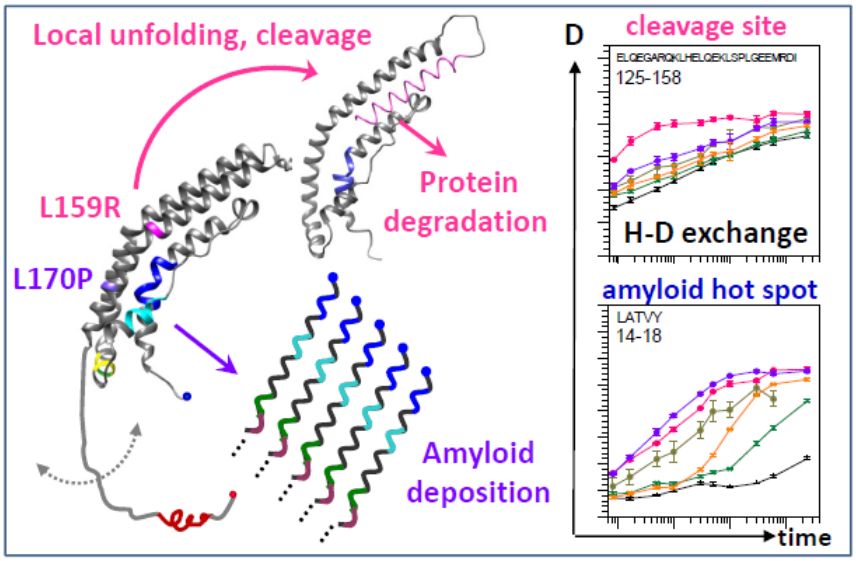

Cover figure legend:

Mutations or post-translational modifications in soluble proteins can lead to pathogenic deposition of amyloid fibrils, yet structural and stability studies of modified proteins often cannot explain why some of them form amyloid in vivo while others do not. Analysis of local and global structure and dynamics in disease-causing mutants of human apolipoprotein A-I, the major protein of "good cholesterol", suggests that increased solvent exposure of amyloidogenic segments together with their presentation in the context of the native helix bundle structure shift the balance from protein degradation to amyloid deposition.

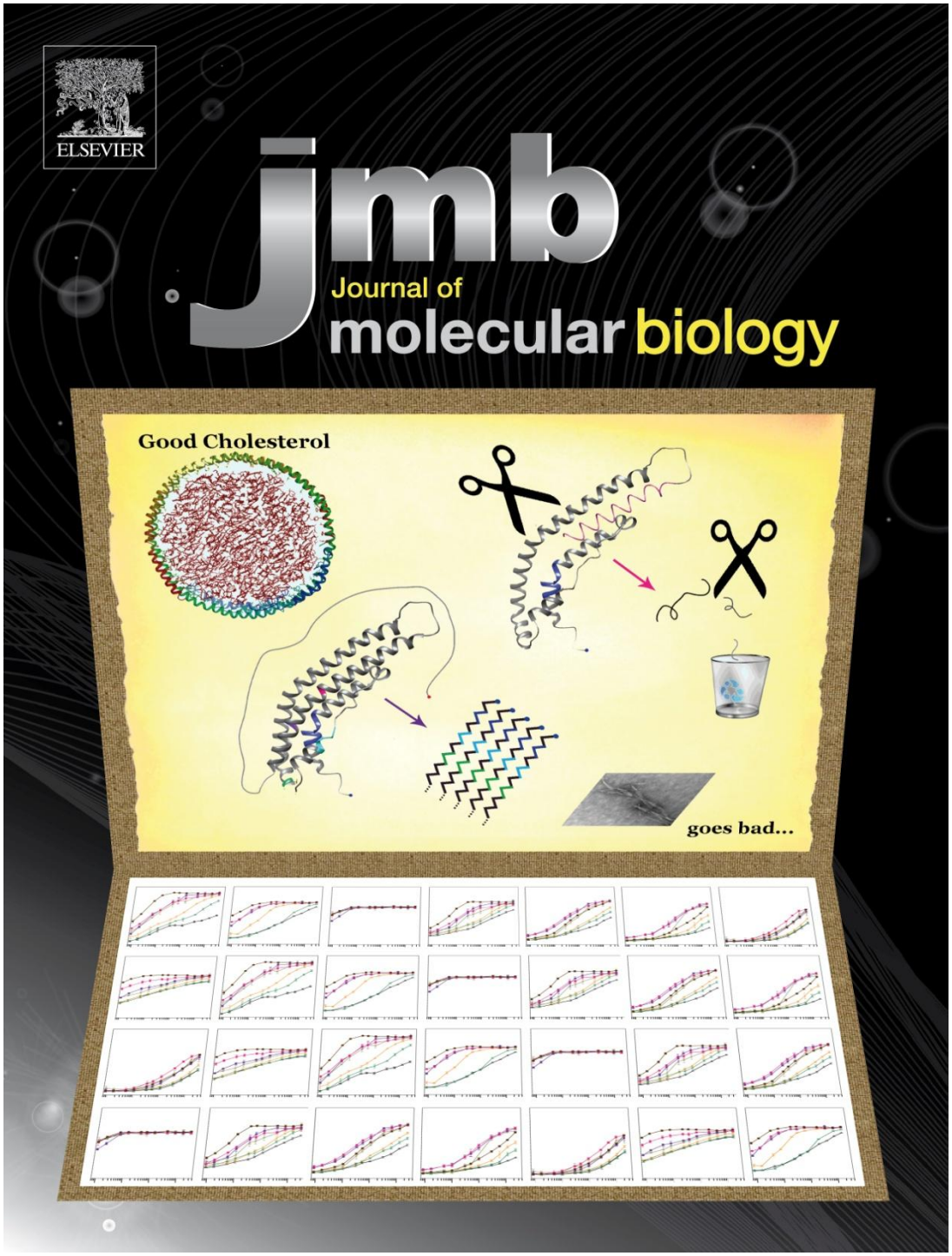

Cover Image

Madhurima Das

Christopher J. Wilson

John R. Engen

Olga Gursky